



## An assessment of aerosol-cloud interactions in marine stratus clouds based on surface remote sensing

Allison McComiskey,<sup>1,2</sup> Graham Feingold,<sup>2</sup> A. Shelby Frisch,<sup>2,3</sup> David D. Turner,<sup>4</sup> Mark A. Miller,<sup>5</sup> J. Christine Chiu,<sup>6,7</sup> Qilong Min,<sup>8</sup> and John A. Ogren<sup>9</sup>

Received 19 August 2008; revised 15 January 2009; accepted 4 February 2009; published 5 May 2009.

[1] An assessment of aerosol-cloud interactions (ACI) from ground-based remote sensing under coastal stratiform clouds is presented. The assessment utilizes a long-term, high temporal resolution data set from the Atmospheric Radiation Measurement (ARM) Program deployment at Pt. Reyes, California, United States, in 2005 to provide statistically robust measures of ACI and to characterize the variability of the measures based on variability in environmental conditions and observational approaches. The average  $ACI_N$  ( $= d\ln N_d/d\ln \alpha$ , the change in cloud drop number concentration with aerosol concentration) is 0.48, within a physically plausible range of 0–1.0. Values vary between 0.18 and 0.69 with dependence on (1) the assumption of constant cloud liquid water path (LWP), (2) the relative value of cloud LWP, (3) methods for retrieving  $N_d$ , (4) aerosol size distribution, (5) updraft velocity, and (6) the scale and resolution of observations. The sensitivity of the local, diurnally averaged radiative forcing to this variability in  $ACI_N$  values, assuming an aerosol perturbation of  $500 \text{ cm}^{-3}$  relative to a background concentration of  $100 \text{ cm}^{-3}$ , ranges between  $-4$  and  $-9 \text{ W m}^{-2}$ . Further characterization of ACI and its variability is required to reduce uncertainties in global radiative forcing estimates.

**Citation:** McComiskey, A., G. Feingold, A. S. Frisch, D. D. Turner, M. A. Miller, J. C. Chiu, Q. Min, and J. A. Ogren (2009), An assessment of aerosol-cloud interactions in marine stratus clouds based on surface remote sensing, *J. Geophys. Res.*, 114, D09203, doi:10.1029/2008JD011006.

### 1. Introduction

[2] The cloud albedo effect is the increase in cloud reflectance that occurs as a result of an increase in aerosol concentration for clouds of equal liquid water [Twomey, 1974, 1977]. The microphysical response associated with the albedo effect is characterized by enhanced cloud drop number concentrations and smaller cloud drop sizes which leads to higher cloud reflectance. Secondary effects of aerosol on clouds are characterized by a suppression of

precipitation [Albrecht, 1989], enhancement in evaporation [Wang *et al.*, 2003; Xue and Feingold, 2006; Jiang *et al.*, 2002], as well as general microphysical-dynamical feedbacks associated with the boundary layer and free-tropospheric cloud system [e.g., Stevens *et al.*, 1998; Ackerman *et al.*, 2004]. The nature and magnitude of these effects are highly uncertain.

[3] Representation of the albedo effect in global-scale climate models has produced a negative (cooling) global, annually averaged radiative forcing estimate of  $-0.7 \text{ W m}^{-2}$  with an uncertainty of  $1.5 \text{ W m}^{-2}$  [Forster *et al.*, 2007]. This radiative forcing carries the greatest uncertainty of all climate forcing mechanisms reported by the Intergovernmental Panel on Climate Change Fourth Assessment Report (IPCC AR4). Radiative forcing, as defined by the IPCC, is the net change in irradiance at the tropopause after stratospheric equilibrium is reached, but with a fixed tropospheric state [Ramaswamy *et al.*, 2001]. Secondary aerosol-cloud effects are consequently relegated by IPCC to feedbacks or “responses” in the climate system as opposed to the “radiative forcing” of the albedo effect [Forster *et al.*, 2007]. Understanding the albedo effect in its own right is required for improving radiative forcing estimates. Therefore, in this paper, we examine aerosol-cloud interactions (ACI) during an intensive observation period at Pt. Reyes, California, United States, to elucidate the mechanisms and uncertainty related to measures of the albedo effect and

<sup>1</sup>Cooperative Institute for Research in Environmental Science, University of Colorado, Boulder, Colorado, USA.

<sup>2</sup>Chemical Sciences Division, Earth System Research Laboratory, NOAA, Boulder, Colorado, USA.

<sup>3</sup>Cooperative Institute for Research in the Atmosphere, Colorado State University, Fort Collins, Colorado, USA.

<sup>4</sup>Space Science and Engineering Center, University of Wisconsin-Madison, Madison, Wisconsin, USA.

<sup>5</sup>Department of Environmental Sciences, Rutgers University, New Brunswick, New Jersey, USA.

<sup>6</sup>Joint Center for Earth Systems Technology, University of Maryland, Baltimore County, Baltimore, Maryland, USA.

<sup>7</sup>NASA Goddard Space Flight Center, Baltimore, Maryland, USA.

<sup>8</sup>Atmospheric Sciences Research Center, State University of New York at Albany, Albany, New York, USA.

<sup>9</sup>Global Monitoring Division, Earth System Research Laboratory, Boulder, Colorado, USA.

implications for local-scale radiative forcing in coastal stratus clouds.

[4] Numerous field studies have corroborated the theory that cloud radiative and/or microphysical properties respond to an increase in aerosol concentrations [Conover, 1966; Ramanathan *et al.*, 2001; Feingold *et al.*, 2003; Twohy *et al.*, 2005, and references therein; Kim *et al.*, 2008]. The existence of the albedo effect is not in question, however, the quantification of this process as it varies under different environmental conditions and with different observational approaches is not well characterized and results in persistent and large uncertainties in forcing. Outstanding questions include: To what extent are various measures of ACI robust and consistent? What are the factors affecting the magnitude of ACI (e.g., cloud type, water phase, dynamics, aerosol composition and size)? Is the variability in metrics of ACI found in the literature due to physical processes, measurement uncertainties, observational approaches, or a combination of all of these?

[5] Aerosol-cloud interactions have been examined empirically using several different variables to represent cloud microphysics (e.g., optical depth, drop effective radius, drop number concentration) and various proxies for aerosol amount (e.g., optical depth, light scattering coefficient, cloud condensation nucleus CCN number concentration). Additionally, these observations have been made from an array of different instruments that reside on various platforms. Measurements are commonly made in situ at the surface or from aircraft and by ground-, aircraft-, and space-based remote sensing. Differences in perspective as well as mismatched sampling in space and time will result in variability and error in the characterization of aerosol-cloud interactions. For a wide range of aerosol concentrations and cloud liquid water, local radiative forcing (under conditions of total cloud cover) can range from approximately  $-1$  to  $-60 \text{ W m}^{-2}$  [McComiskey and Feingold, 2008]. Understanding the relationships among these various measures is a necessary first step toward understanding the natural variability of the processes in different environmental conditions as distinct from measurement error. A quantitative characterization of aerosol-cloud interactions on process-level scales is necessary for reducing the uncertainty in associated radiative forcing estimated by global-scale climate models.

[6] Here we focus on variability and uncertainty in ACI measures and the resulting radiative forcing from ground-based remote sensing observations under coastal stratus cloud. These clouds are typically characterized by lower liquid water and drop number concentrations than more highly convective cloud types, and have been shown to be more susceptible (in terms of an albedo response) to changes in aerosol [Platnick and Twomey, 1994]. Kim *et al.* [2003] suggested that the less complex meteorological conditions in which they exist may also predispose stratus to an enhanced albedo response. Their complete cover provides for continuous measurement of cloud microphysical properties from remote sensing without the 3D radiative effects of broken clouds [Barker, 2000; Kassianov *et al.*, 2005]. Ground-based remote sensing and in situ observations are used to examine aerosol-cloud interactions during the Pt. Reyes study within nonprecipitating clouds only, to avoid ambiguities in the relationships between aerosol and

cloud microphysics. Some comparisons with airborne in situ observations are presented in comparison to ground-based observations. Finally implications for uncertainties in estimating the radiative forcing of the albedo effect will be presented. While aerosol-cloud interactions have implications for longwave radiative forcing [e.g., Lubin and Vogelmann, 2006], we only address shortwave radiative forcing.

## 2. Framework for Calculations

[7] The microphysical component of the albedo effect can be detected using several related cloud microphysical properties: cloud optical depth  $\tau_d$ , cloud drop effective radius  $r_e$ , and cloud drop number concentration  $N_d$ . As aerosol concentration increases,  $N_d$  increases and  $r_e$  decreases, thus increasing  $\tau_d$  through stronger backscattering from more, and smaller cloud droplets (for a constant cloud liquid water path (LWP)). The albedo effect, expressed as  $ACI_x$ , where  $x \in \{\tau, r, N\}$  (representing  $\tau_d$ ,  $r_e$ , and  $N_d$ , respectively) can be defined by the following equalities [Feingold *et al.*, 2001]:

$$ACI_\tau = \left. \frac{\partial \ln \tau_d}{\partial \ln \alpha} \right|_{LWP} \quad 0 < ACI_\tau < 0.33 \quad (1a)$$

$$ACI_r = - \left. \frac{\partial \ln r_e}{\partial \ln \alpha} \right|_{LWP} \quad 0 < ACI_r < 0.33 \quad (1b)$$

$$ACI_N = \frac{d \ln N_d}{d \ln \alpha} \quad 0 < ACI_N < 1.0 \quad (1c)$$

$$ACI_\tau = -ACI_r = \frac{1}{3} ACI_N \quad (1d)$$

where  $\alpha$  is an observed proxy for aerosol amount. Note that  $ACI_\tau$ ,  $ACI_r$ , and  $ACI_N$  values are bounded by 0–0.33, 0–0.33, and 0–1.0 respectively, reaching the maximum absolute values if all aerosol particles are activated to droplets. We use the term “ACI” rather than “albedo effect” or “indirect effect” to differentiate the fact that the ACI metrics are associated with microphysical responses, rather than radiative forcing.

[8] Theoretical relationships among the above variables,  $r_e \propto \text{LWP}/\tau_d$  [Stephens, 1978] and  $\tau_d \propto N_d^{1/3}$  (at constant LWP) [Twomey, 1977], yield the equalities found in equation (1). However, robust empirical assessment of the magnitude of ACI, and the extent to which measurements conform to equation (1) over a range of environmental conditions is still lacking. Studies of this nature are required to reduce uncertainties in estimating the radiative forcing due to the albedo effect. Also lacking is the reconciliation of these measures across scales that result from observations on various platforms. We use independent observations of aerosol together with cloud microphysical properties derived from different methods to assess the magnitude of ACI and the extent to which these empirical measures are consistent with equation (1d).

[9] We stress that this is a simplified representation of the activation process and that other parameters such as aerosol size, composition, and updraft velocity  $w$ , also play a role in

**Table 1.** Cloud and Aerosol Properties Measured or Derived From Observations at Pt. Reyes, California

Measured Quantity	Definition	Instrument(s)
Cloud liquid water path	LWP ( $\text{g m}^{-2}$ )	MWR
Cloud optical depth	$\tau_d$	2NFOV
Cloud drop effective radius	$r_e$ ( $\mu\text{m}$ ) = $1.5(\text{LWP}/\tau_d)^a$	2NFOV/MWR
Cloud updraft velocity	$w$ ( $\text{m s}^{-1}$ )	Doppler radar
Total aerosol light Scattering	$\sigma_s$ ( $\text{Mm}^{-1}$ )	TSI nephelometer
Ångström exponent	$\dot{a} = -\log[\sigma_s(\lambda_1)/\sigma_s(\lambda_2)]/\log(\lambda_1/\lambda_2)$	TSI nephelometer
Aerosol index	AI ( $\text{Mm}^{-1}$ ) = $\sigma_s \times \dot{a}$	TSI nephelometer
Cloud condensation nucleus concentration	$N_{\text{CCN}}$ ( $\text{cm}^{-3}$ ) at $S = 0.55\%$	DMT CCN counter
Cloud drop number concentration	$N_d$ ( $\text{cm}^{-3}$ ) = $C(T, P)\tau_d^3\text{LWP}^{-2.5}$ b	MWR/2NFOV

<sup>a</sup>Stephens [1978].

<sup>b</sup> $C(T, P)$  = a known function of cloud base temperature  $T$  and pressure  $P$ ; relationship based on adiabatic assumption.

determining the ultimate magnitude of the Twomey effect. For example, Liu and Daum [2002] show that enhanced aerosol concentrations work to increase the dispersion of the cloud drop size distribution, which reduces the Twomey effect. While the importance of aerosol size and  $w$  to calculated ACI values are considered in section 4.2, they are not explicitly represented in the ACI calculations. The definitions of ACI in equation (1) and the theoretical bounds they assume primarily account for the effect of perturbations in aerosol concentration alone, however, the above factors may influence the magnitude of the albedo effect to a greater or lesser extent. Omission of one or several of these other factors may explain “invalid” ACI values, or those that fall outside of the stated bounds set forth in equation (1), a condition that is sometimes encountered in the analyses presented here.

[10] ACI is presented in each of the forms in equation (1) throughout the paper and the relevant form is indicated by the appropriate subscript ( $\tau$ ,  $r$ ,  $N$ ) to remind the reader of the appropriate range into which the individual results fit. When examining the sensitivity of ACI to other variables, the form  $\text{ACI}_N$  is often used for simplification because the  $N_d - \alpha$  relationship focuses on activation and has no fundamental microphysical relationship to LWP, except indirectly through correlations between cloud turbulence and LWP. In reality, however,  $N_d$  is derived from LWP as discussed below, so that interpreting results achieved by sorting clouds by their LWP requires caution.

### 3. Observations From Pt. Reyes, California

[11] The Department of Energy Atmospheric Radiation Measurement (ARM) Program’s deployment of the ARM Mobile Facility (AMF) in 2005 at Pt. Reyes, California (N 38° 5.46′ W 122° 57.43′) [Miller and Slingo, 2007] provided a rich data set for assessing aerosol effects on coastal stratus. The deployment ran from mid-March through mid-September 2005 on the ground, with a coordinated airborne campaign, the Marine Stratus Radiation Aerosol and Drizzle (MASRAD) Intensive Observation Period (IOP) during the month of July.

[12] The aerosol and cloud properties required for quantifying ACI as in equation (1) were available at Pt. Reyes from a suite of instruments and are summarized in Table 1. Analyses depend strongly on an accurate record of cloud LWP that was made by a microwave radiometer (MWR) [Turner et al., 2007]. LWP observations suffered from a wet window problem earlier in the field deployment, therefore

only data from late June through September are used here. LWP observations below  $50 \text{ g m}^{-2}$  were excluded to avoid very thin or broken cloud cover, as well as postprecipitation conditions. Observations above  $\sim 150 \text{ g m}^{-2}$  were excluded to avoid the bulk of precipitating clouds, although some cloud with LWP lower than  $\sim 150 \text{ g m}^{-2}$  may have precipitated to some lesser extent. In selected cases, a larger LWP range,  $50 - 300 \text{ g m}^{-2}$ , is used to illustrate the effect of drizzle on ACI. Uncertainty in the MWR-retrieved LWP is approximately  $15 \text{ g m}^{-2}$  for the range of values encountered at Pt. Reyes [Turner et al., 2007]. Cloud optical depth,  $\tau_d$ , was retrieved from the two-channel Narrow Field-of-View radiometer (2NFOV) at 1-s resolution [Chiu et al., 2006] and  $r_e$  was derived from  $\tau_d$  and LWP as in Table 1.  $N_d$  was derived from LWP and  $\tau_d$  using the adiabatic assumption:

$$N_d = C(T, P)\tau_d^3\text{LWP}^{-2.5}, \quad (2)$$

where  $C(T, P)$  is a known function of temperature  $T$  and pressure  $P$ . Where indicated, Twomey’s semianalytical function [Twomey, 1959] is also used:

$$N_{d,T} = c^{1-[k/(k+2)]} \left[ \frac{f_1(T, P)w^{3/2}}{f_2(T, P)f_3(T, P)kB(3/2, k/2)} \right]^{k/(k+2)}, \quad (3)$$

where  $c$  and  $k$  are related to the concentration and slope of a Junge aerosol size distribution, (or equivalently, the fit parameters of a supersaturation activation spectrum),  $B$  is the beta function,  $w$  the updraft velocity, and  $f_{1,2,3}(T, P)$  thermodynamic functions of  $T$  and  $P$ . Equation (2) is based on knowledge of LWP and  $\tau_d$ , while equation (3) also assumes adiabaticity and requires knowledge of CCN parameters and  $w$  (measured here by a vertically pointing Doppler cloud radar). Equation (3) is inherently a more stable retrieval of  $N_d$  than equation (2) because it is strongly dependent on aerosol parameters ( $c$ ,  $k$ ) that tend to change relatively smoothly. Use of equation (2) can become unstable at times because it depends directly on two measured cloud parameters with their inherent errors.

[13] Note that corrections to equations (2) and (3) to account for subadiabaticity can be applied ( $N'_d = \beta^{1/2}N_d$ , where  $\beta$  is the ratio of LWP to the adiabatic LWP) but have not been made because of the general difficulty in determining cloud base  $T$  when soundings are unavailable. However, the fact that these clouds are known to achieve liquid water contents that are close to adiabatic [e.g.,

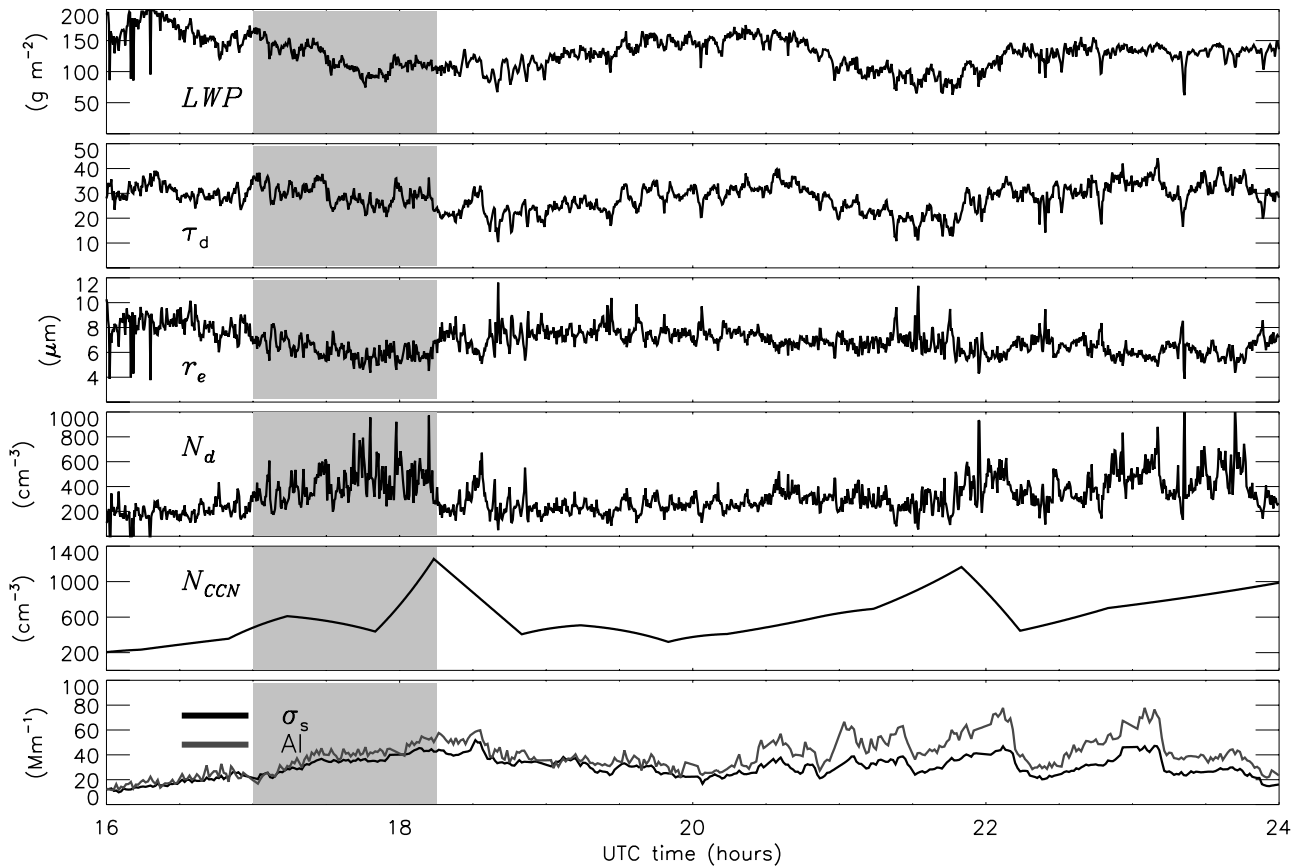


**Figure 1.** A subset of data from 3 September 2005 for each of the aerosol and cloud properties used in the aerosol-cloud interactions (ACI) calculations for the AMF Pt. Reyes deployment. All of the variables are interpolated to a common 20-s time stamp dictated by the frequency of liquid water path (LWP) observations. The shaded area illustrates the effect of aerosol on cloud microphysics with the increase in aerosol ( $N_{CCN}$ ,  $\sigma_s$ , AI) accompanied by an increase in  $N_d$ , and a decrease in  $r_e$ . The decreasing LWP over this period, accompanied by the changes in  $N_d$  and  $r_e$ , results in an approximately constant  $\tau_d$ .

Brenguier *et al.*, 2003] suggests that this will not significantly affect the empirical relationships from these large data sets. All cloud parameters are interpolated to the 20-s temporal resolution of the MWR, which is used as a base resolution to which all other properties are interpolated and time-synchronized.

[14] Note that whereas some previous studies have used radar and microwave radiometer retrievals of  $r_e$  that are not limited by time-of-day, the current study relies on  $\tau_d$  measurements for all of  $ACI_{\tau}$ ,  $ACI_r$ , and  $ACI_N$ . We therefore limit our analysis to daylight hours and reasonably high solar zenith angles. The relative merits of radar reflectivity versus  $\tau_d$  retrievals of  $r_e$  are discussed by Feingold *et al.* [2006].

[15] To represent aerosol, in situ observations at the surface from the Aerosol Observation System (AOS) [Sheridan *et al.*, 2001; Delene and Ogren, 2002] were used. At Pt. Reyes throughout the time period of analysis, a well-mixed boundary layer ensured that surface observations were representative of the aerosol aloft and that interacted with cloud. The AOS takes in air from a tower over the site for in situ sampling of several aerosol optical properties and is heated to obtain measurements at a relative humidity of no more than 40%. Total aerosol light scattering  $\sigma_s$  is

measured by an integrating nephelometer (TSI Model 3563) at wavelengths of 450, 550, and 700 nm. Scattering at 550 nm is used here while the spectral information is used to determine an Ångström exponent  $\hat{a}$  (Table 1);  $\hat{a}$  is related to the shape of the aerosol size distribution and can be used as a proxy for aerosol size information and is, in fact, also proportional to  $k$  in equation (3). From these measurements the aerosol index AI, the product of the scattering and Ångström exponent, is calculated. Nakajima *et al.* [2001] suggested that ACI may be more sensitive to AI than measures of aerosol optical depth alone, owing to increased sensitivity to particle size. Uncertainties in the aerosol light scattering measurements are approximately 10% for the magnitude of scattering at Pt. Reyes [Jefferson, 2005; Anderson *et al.*, 1999].

[16] Aerosol optical properties were originally collected at 1-min resolution on a 30-min cycle that oscillates between  $< 10 \mu\text{m}$  and  $< 1 \mu\text{m}$  aerosol particle diameter size cuts. For this study we use the  $< 10 \mu\text{m}$  size cut data and interpolate across the 30-min gaps, using the variability information in the  $< 1 \mu\text{m}$  aerosol observations to produce a continuous 1-min temporal resolution time series of each aerosol property. This continuous 1-min resolution data set is then interpolated to the base 20-s resolution of the MWR.

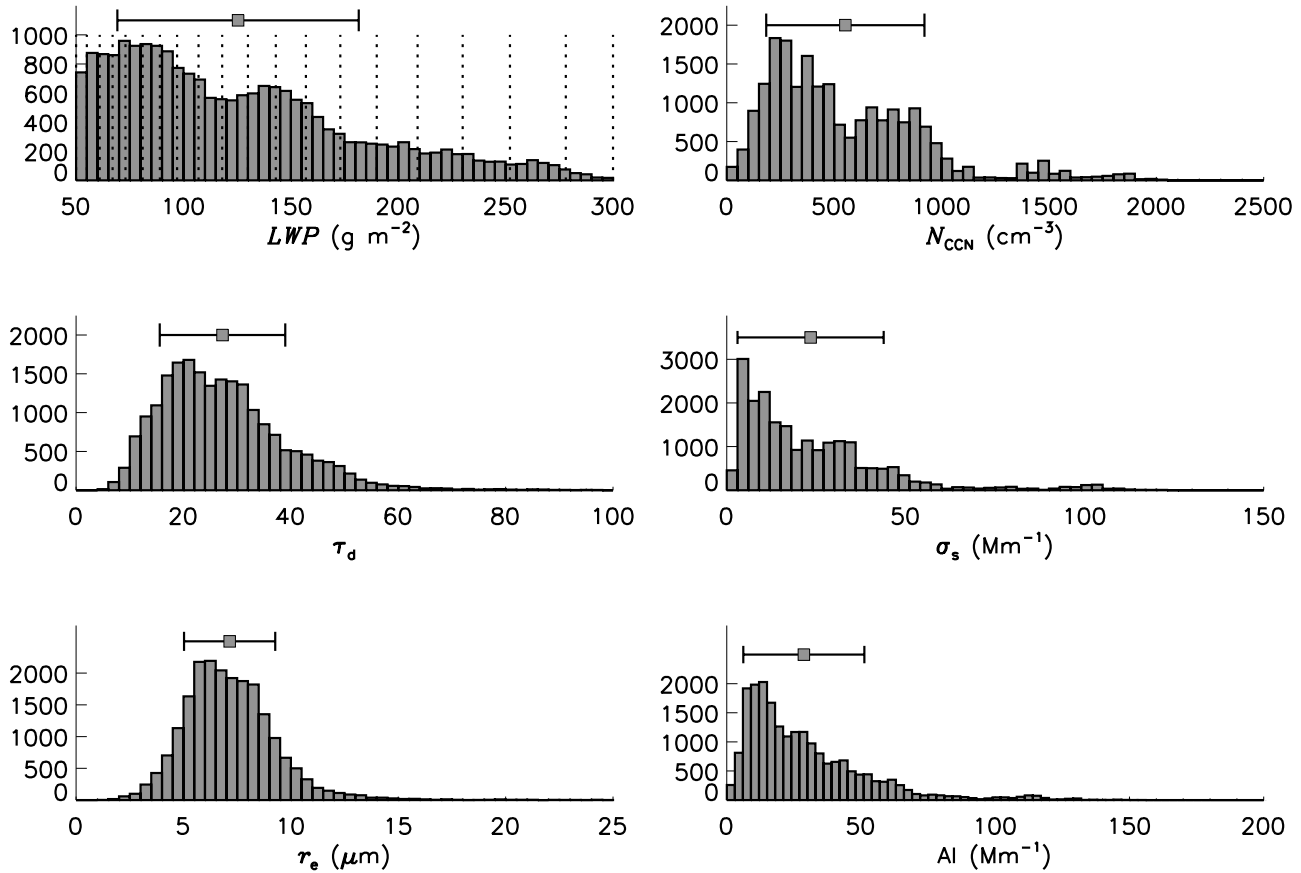


**Figure 2.** Histograms of observed aerosol and cloud properties over the Pt. Reyes deployment. The square symbols above the histograms represent the mean, and the bars represent one standard deviation from the mean.

[17] A CCN counter by Droplet Measurement Technologies, Inc. (DMT) measured CCN number concentration  $N_{\text{CCN}}$ , by scanning through a range of supersaturations (0.18 – 1.37%) every 30 min. By definition, the size of the aerosol particles that are activated varies by supersaturation with the largest particles being activated at the lowest supersaturations for a given solubility. Interpolated CCN data are produced on the basis of the relationship between the measured CCN concentrations with increase in supersaturation,  $S$ :  $N_{\text{CCN}} = cS^k$  [Twomey, 1959], where fit parameters  $c$  and  $k$  (equation (3)) are calculated for each 30-min scan.  $N_{\text{CCN}}$  is calculated on the basis of a given  $S$  of 0.55% for each half hour and these values are interpolated down to 20-s resolution. This method of interpolating the CCN data does not preserve the higher temporal variability of the 1-min aerosol optical properties and is dependent on a prescribed  $S$ . While cloud microphysical properties can vary on the short timescales that we examine here, aerosol properties tend to vary on relatively longer timescales [Anderson *et al.*, 2003], therefore the reduction in resolution of the aerosol data will not likely affect the sensitivity of the calculations of ACI.

[18] Figure 1 shows a subset of the variables used in ACI calculations from Pt. Reyes on September 3, 2005 at 20-s resolution. This particular time period illustrates the effect of aerosol on cloud microphysics exceptionally well. Cloud optical depth tracks the LWP to first order, as expected

[Schwartz *et al.*, 2002], but some variability in the relationship exists. A proportion of this variability in  $\tau_d$  can be explained by the effects of changing aerosol concentrations. As aerosol concentration increases (shaded area around 1700 to 1815 UTC),  $r_e$  is seen to decrease. Isolated, ideal events such as these have often been used to quantify ACI. In order to generalize a quantified theory for inclusion into models, analyses are required that bridge temporal scales. The high-resolution, continuous time series of data from the ground-based measurements at Pt. Reyes provide a statistically robust data set for examination of ACI at different temporal scales. Here, data from the full field deployment are used in aggregate as well as for shorter timescales to assess the consistency of expected ACI measures in equation (1) across sampling scales for coastal stratus.

[19] Aggregate statistics for the Pt. Reyes field deployment are presented in Figure 2 as frequency histograms for each property used in ACI calculations. The mean and standard deviation of the properties are indicated above each histogram. Of course, observed variability in aerosol loading is required to detect the albedo effect. While the aerosol in general exhibits little variability on a daily basis, the data from the full deployment provides sufficient variability for quantifying ACI. The implicit assumption in deriving ACI from the aggregate data is that aerosol size distribution and composition are less important than aerosol number concentration in determining  $N_d$ . This has been

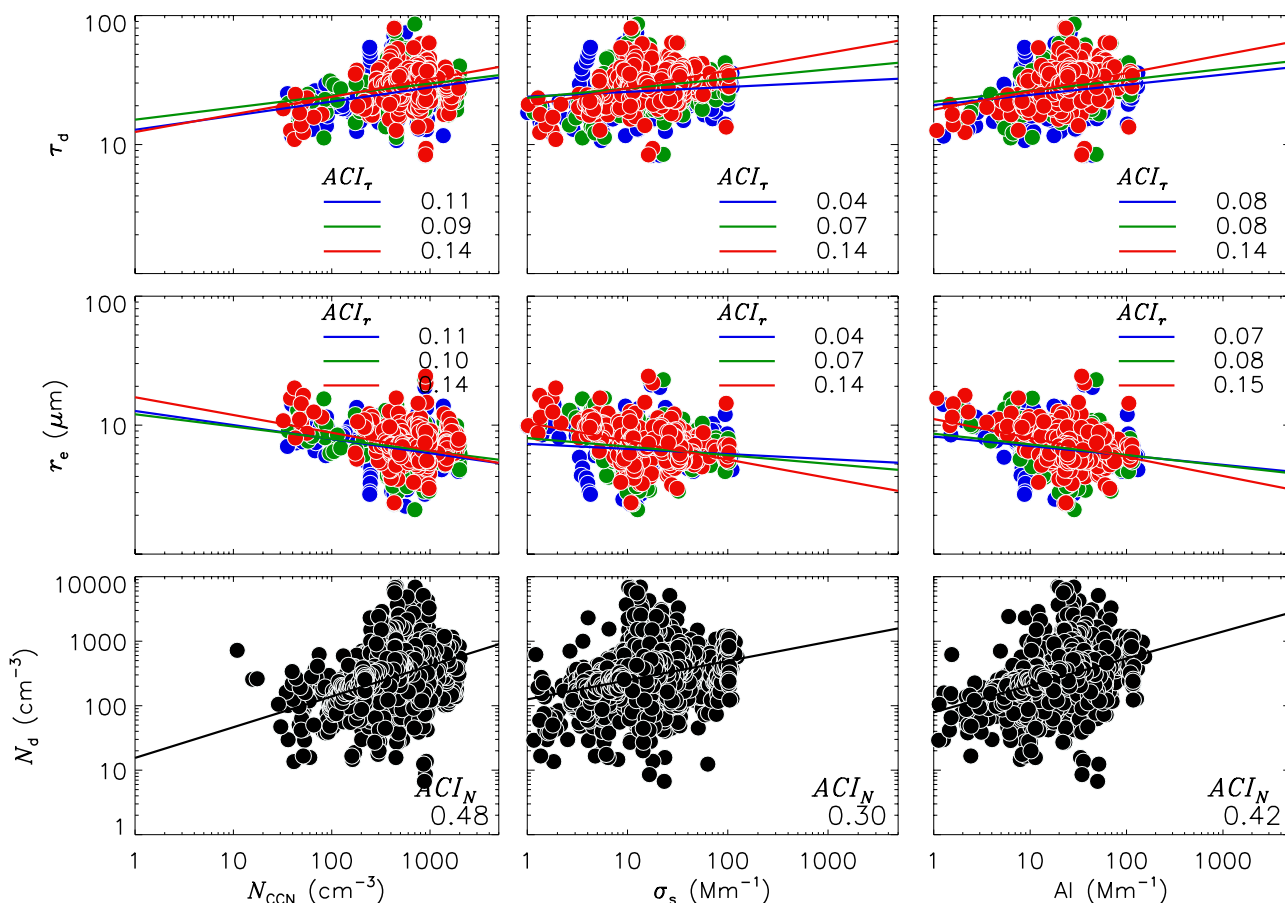


**Figure 3.** Measures of ACI from equation (1) sorted by LWP and showing expected consistency among the different measures. Cloud properties ( $\tau_d$ ,  $r_e$ ,  $N_d$ ) are derived from measurements made by the 2NFOV and MWR instruments, and aerosol properties ( $N_{CCN}$ ,  $\sigma_s$ , Al) are derived from ground-based in situ observations made by the Aerosol Observation System (AOS). Regressions are made for LWP bins geometrically increasing in size by 10% around an approximate mean LWP value ( $120 \text{ g m}^{-2}$ ) for the deployment. Regressions shown are for the following bins: blue,  $107 \leq \text{LWP} < 118 \text{ g m}^{-2}$ ; green,  $118 \leq \text{LWP} < 130 \text{ g m}^{-2}$ ; and red,  $130 \leq \text{LWP} < 143 \text{ g m}^{-2}$ .

shown to be the case for relatively clean marine environments [Feingold, 2003]. The number of observations for the aggregate data set is approximately 21,000. In the next section we present the analysis of these data in aggregate followed by data sampled from shorter time periods.

## 4. Results and Discussion

### 4.1. Aggregate Results

#### 4.1.1. ACI Measures

[20] ACI is calculated for the aggregate ground-based data from the Pt. Reyes deployment (Figure 3) using the available cloud ( $\tau_d$ ,  $r_e$ ,  $N_d$ ) and aerosol ( $N_{CCN}$ ,  $\sigma_s$ , Al) observations. An accurate quantification of the albedo effect requires that cloud LWP be held constant so that changes in available liquid water do not confound changes in cloud reflectance caused by increasing aerosol and decreasing drop sizes [Twomey, 1974; Schwartz *et al.*, 2002]. Calculations of  $ACI_r$  and  $ACI_\tau$  are made by sorting  $\tau_d$ ,  $r_e$ , and the aerosol properties into 10% increasing LWP bins (i.e., bin bounds are defined by  $\text{LWP}_{i+1} = 1.10 \times \text{LWP}_i$ ) over the  $50 - 157 \text{ g m}^{-2}$  range (the upper limit of the range at  $157 \text{ g m}^{-2}$  is that of the full 10% LWP bin including the assumed

precipitation threshold of  $\sim 150 \text{ g m}^{-2}$ ). The number of observations falling into each bin is indicated in Figure 2 by the dashed lines. Only several of the bins are shown in Figure 3 for  $ACI_\tau$  and  $ACI_r$ . Since  $N_d$  is calculated as a function of LWP the full aggregate data set is represented by the values shown for  $ACI_N$ .

[21] The range of values for  $ACI_r$ , 0.05–0.16, is broadly consistent with previous findings from ground-based remote sensing in stratiform clouds. Kim *et al.* [2008] found  $ACI_r$  values between 0.04 and 0.17 in continental stratus from a 3-year study over the DOE ARM Southern Great Plains site in Oklahoma. At the same site, Feingold *et al.* [2003] derived  $ACI_r$  values of 0.02–0.16 for a set of seven cases. In the Arctic, Garrett *et al.* [2004] found  $ACI_r$  of 0.13–0.19 from similar instrumentation as was used here. Airborne, in situ, campaigns in stratiform clouds at several different locations [Ramanathan *et al.*, 2001 and references therein] produce an  $ACI_N$  range of 0.63–0.99 (an  $ACI_r$  range of 0.21–0.33) for a broad range of aerosol concentrations including very high concentrations. Measurements off the California coast in the Dynamics and Chemistry of Marine Stratocumulus-II experiment resulted in equivalent  $ACI_r$  of 0.27 [Twohy *et al.*, 2005]. Similar ranges have been found

**Table 2.** ACI and Statistical Parameters, Pearson Product-Moment Correlation Coefficient,  $r$ , and the Coefficient of Determination,  $r^2$ , for the Aggregate Pt. Reyes Data

	$N_{CCN}$	$\sigma_{sp}$	AI
$ACI_{\tau_r}$ <sup>a</sup> (n = 1,310) <sup>b</sup>	0.16	0.08	0.14
$r$	0.37	0.24	0.39
$r^2$	0.14	0.06	0.15
$ACI_N$ (n = 20,996)	0.48	0.30	0.42
$r$	0.37	0.25	0.39
$r^2$	0.14	0.06	0.15

<sup>a</sup>Statistics for aerosol-cloud interactions ( $ACI_r$ ) and  $ACI_r$  are identical because of the relationship of  $r_e$  to  $\tau_d$  (Table 1).

<sup>b</sup>Average number of observations within all LWP bins.

from space-based remote sensing derivations of  $ACI_r$  (0.01–0.19) [Nakajima *et al.*, 2001; Bréon *et al.*, 2002; Chameides *et al.*, 2002; Quaas *et al.*, 2004], although they tend toward lower values on average, possibly because data are not stratified by LWP.

[22] When ACI values are averaged over all LWP bins the ACI measures are consistent among all three forms, as expected. The average values over all LWP bins are presented in Table 2 with the Pearson product-moment correlation coefficient,  $r$ , and the coefficient of determination,  $r^2$ . The slopes of each of the nine measures of ACI presented here are significant at a 99% probability level based on a student’s  $t$  test, owing to the large number of samples from which they are calculated.

[23] The three cloud microphysical properties presented are not all independent measurements, which explains some of the consistency observed across measures. For example, the relationship  $r_e \sim \text{LWP}/\tau_d$  ensures that  $ACI_r$  and  $ACI_\tau$  are the same if data are sorted by LWP. This provides verification that cloud microphysical properties derived as per the relationships in Table 1 can be used interchangeably when examining aerosol-cloud interactions. Note however that  $ACI_\tau$  does constitute a set of three independent measures ( $\tau_d$ , LWP and  $\alpha$ ) and as such is the preferred way to derive ACI for this study, all else being equal. In general,  $ACI_\tau$  is also preferred because it provides a more direct link to the cloud radiative response by which the Twomey effect is defined owing to the relationship between  $\tau_d$  and albedo. As stated in section 2, we present results in several cases in the form of  $ACI_N$  (avoiding the necessity of sorting by LWP) in order to simplify the presentation when sorting by variables other than LWP. Within the aerosol measurements  $N_{CCN}$  and  $\sigma_s$  are independent.

[24] An examination of the correlation coefficient shows that a stronger association exists between CCN concentrations and changes in cloud microphysics,  $r = 0.37$ , than for aerosol light scattering,  $r = 0.25$ , despite the fact that the scattering data are collected at a higher temporal resolution. Consideration of the aerosol size information using AI increases the association to  $r = 0.39$ . The ability to substitute AI as a proxy for direct CCN measurements without loss of sensitivity to ACI is extremely useful since multiwavelength light scattering measurements are widely available. The coefficient of determination,  $r^2$ , suggests that between 6% and 15% of the variability in cloud microphysical properties may be explained by changes in aerosol concentrations for the different proxies presented.

#### 4.1.2. Dependence on LWP

[25] While the averaged values for ACI are consistent within the different forms, individual values over the range of LWP bins vary considerably (Figure 3). Over the range of LWP for stratiform clouds at Pt Reyes, 50 – 300  $\text{g m}^{-2}$ , which may include nonprecipitating and precipitating clouds, no dependence of ACI calculated for the 10% increasing LWP bins is found (Figure 4). However, if only lower LWPs (<150  $\text{g m}^{-2}$ ) are considered, representing clouds that are most likely nonprecipitating, a reduction in ACI with increasing LWP is clear. To explore the reasons for this trend, we consider the fact that, all else being equal, an increase in LWP is accompanied by an increase in drop collision-coalescence and reduction in  $N_d$ . The right ordinate of Figure 4 shows that, as expected,  $N_d$  decreases with increasing LWP. Therefore collision-coalescence likely obscures the magnitude of ACI associated with drop activation at the higher LWPs. Even in the absence of precipitation there is a need to consider the effect of processes other than activation on ACI. At  $\text{LWP} > \sim 150 \text{ g m}^{-2}$  and in the presence of precipitation, aerosol is scavenged from the atmosphere, resulting in highly variable, and even negative ACI (Figure 4) possibly due to the small range of aerosol concentration. The effects of a limited range of aerosol concentration on calculating ACI are examined later in section 4.3 and Figure 11.

[26] If the constraint of constant LWP is ignored, large differences in calculated ACI can occur if a significant range in LWP exists. Variations in  $\tau_d$  driven by processes other than increased aerosol concentrations will also drive variation in LWP and will decrease the sensitivity of equation (1) if an analysis lumps all LWP values. This is illustrated in Figure 5. The aggregate data from Pt. Reyes show that for “lumped” LWP (all data with LWP ranging

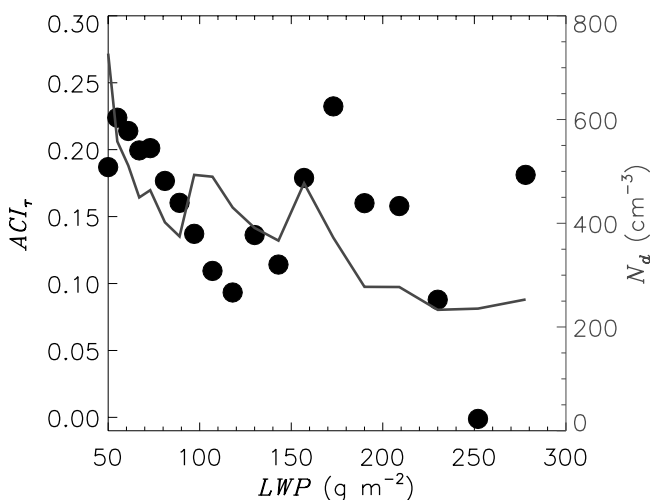


**Figure 4.** Relationship of (symbols, left ordinate)  $ACI_\tau$  and (line, right ordinate)  $N_d$  to increasing LWP.  $ACI_\tau$  is calculated for 10% increasing LWP bins in the range of 50–300  $\text{g m}^{-2}$  and  $N_d$  derived using equation (2). Note the general reduction in  $N_d$  with increasing LWP for values <  $\sim 150 \text{ g m}^{-2}$ , and highly variable  $ACI_\tau$  for  $\text{LWP} > \sim 150 \text{ g m}^{-2}$ . Under the latter conditions,  $ACI_\tau$  is more reflective of scavenging processes than aerosol effects on cloud microphysics.

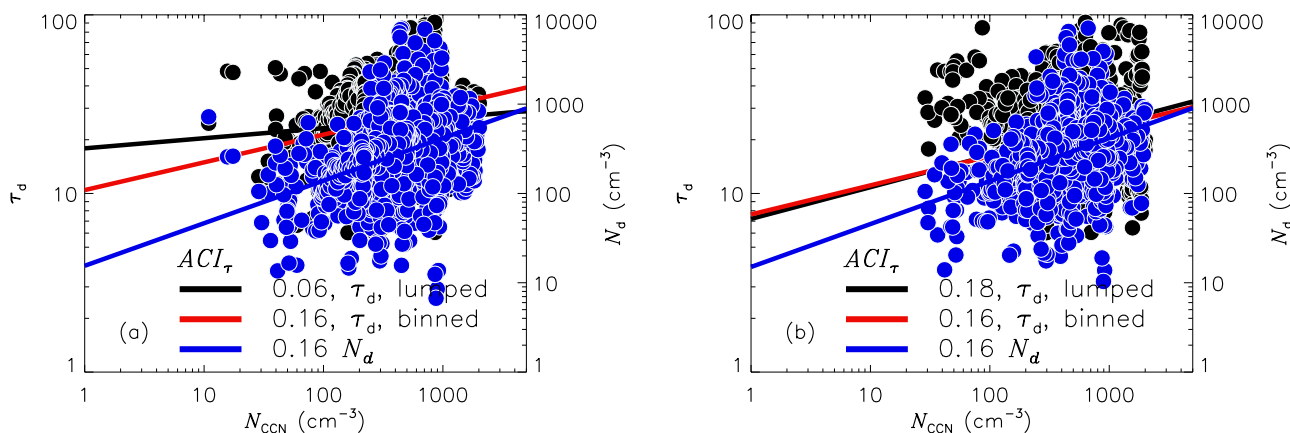


**Figure 5.** The difference in ACI for the aggregate Pt. Reyes data that is (black) lumped versus (red) binned by LWP for a LWP range of (a) 50–300  $\text{g m}^{-2}$  and (b) 50–157  $\text{g m}^{-2}$ . The  $ACI_\tau$  value for  $N_d$  represents  $1/3 ACI_N$ ;  $ACI_N = 0.48$  for the aggregate data set for both ranges of LWP in Figures 5a and 5b.

from 50 to 300  $\text{g m}^{-2}$ ),  $ACI_\tau = 0.06$  whereas for the data sorted into LWP bins the average ACI among the bins is 0.16. If the LWP range is limited to lower values (all data with LWP ranging from 50 to 157  $\text{g m}^{-2}$ ), as in Figure 5b, the lumped  $ACI_\tau = 0.18$ , is similar to the value of the binned data. This finding has important implications for measurements used in characterizing ACI that have vastly different scales and resolutions. For example, a sensor with a large spatial footprint or temporal averaging period precludes the ability to sort by LWP, leading to biases in ACI. This concept is further illustrated in section 4.3.

#### 4.1.3. $N_d$ Retrievals

[27] Differences in retrieval methods for aerosol and cloud properties can contribute to uncertainty in ACI. Variation in ACI for  $N_d$  derived by three common approaches is shown in Figure 6. In situ airborne observations from the Marine Airborne Stratocumulus Experiment (MASE) of  $N_d$  were collected over the Pt. Reyes field site in July 2005 [Lu et al., 2007] resulting in an  $ACI_N$  value of 0.56. The values from the ground-based data set are 0.52 for the  $N_d$  (adiabatic, equation (2)) and 0.43 for the  $N_{d,T}$  (Twomey, equation (3)) retrievals. Despite some temporal mismatch in the two data sets, the average  $ACI_N$  values between the airborne and ground-based observations are comparable.

[28] Boers et al. [2006] and Bennartz [2007] showed that space-based remote sensing, using the MODIS sensor, could be used to reliably monitor  $N_d$  concentration and its relationship to cloud albedo and cloud geometric thickness. The results in Figure 6 are the first evidence that ground-based remote sensing can also provide robust measurement of aerosol effects on cloud microphysics in (close-to-) adiabatic clouds. Use of an independent and directly measured microphysical property, such as  $\tau_d$  in the case of the Pt. Reyes deployment, is preferred for assessing aerosol-cloud interactions (for reasons described above), however, these results indicate that  $ACI_N$  derived from different  $N_d$  retrievals shows consistency with ACI derived from optical depth observations and can be used when more direct measurements are not available, provided clouds are close-to-adiabatic.

#### 4.2. Natural Drivers of ACI Variability

[29] The values for ACI in Figure 3 are physical and consistent with other observations, yet are somewhat less than what might be expected according to common assumptions regarding the number of particles within a population that become activated. Twomey [1974] provided a rough estimate of  $ACI_N = 0.8$ , Pruppacher and Klett [1997] and Feingold [2003] suggested  $ACI_N = 0.7$ , while the observations from Pt. Reyes are closer to  $ACI_N = 0.5$ . Studies have shown that ACI is sensitive to natural variability in aerosol properties such as concentration, size and chemistry [Feingold et al., 2001], cloud dynamical processes [Kim et al., 2008] and other meteorological parameters such as updraft velocity [Feingold et al., 2003]. Dusek et al. [2006] found that the aerosol size distribution accounted for approximately 90% of the variability in activated CCN concentrations, with little influence due to composition. Modeling by Feingold [2003] and Ervens et al. [2005] showed that for internally mixed aerosol, composition has a relatively small effect on droplet activation, except perhaps under very

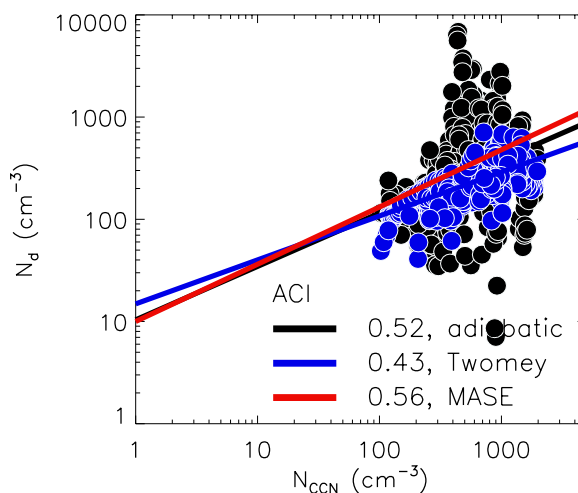


**Figure 6.** Differences in  $ACI_N$  for various retrievals of cloud drop number,  $N_d$ , from ground-based remote sensing and in situ airborne observations.

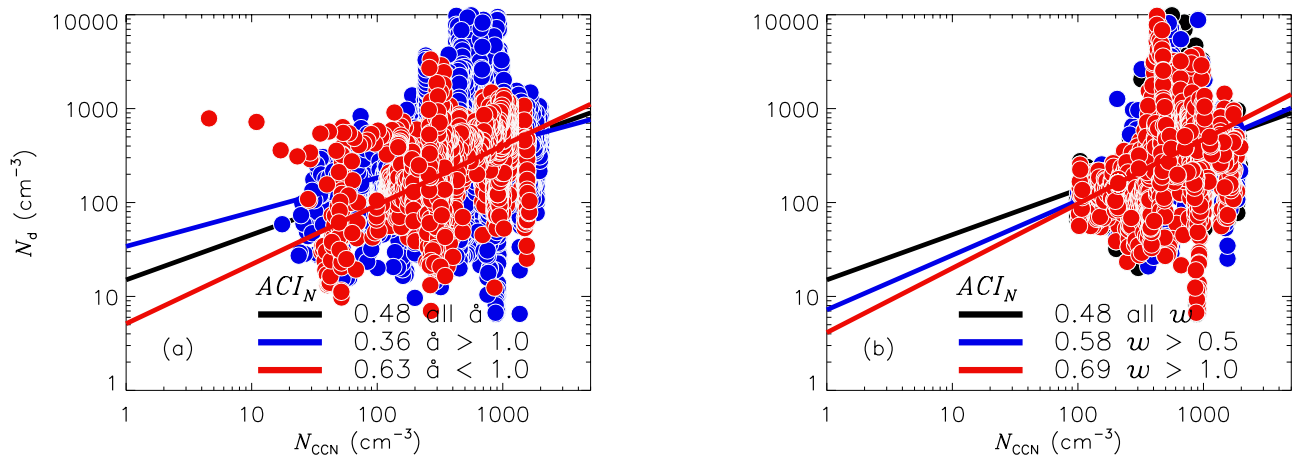


**Figure 7.** Differences in ACI for naturally varying parameters (a) Ångström exponent  $\hat{a}$  and (b) updraft velocity  $w$  (in  $\text{m s}^{-1}$ ).

polluted conditions and small  $w$ . Sensitivity to these factors, and others is explored below.

#### 4.2.1. Activation and Collision-Coalescence

[30] It has been shown here that in addition to the above factors, one must also consider the influence of drop-drop interactions such as collision-coalescence (Figure 4). By reducing  $N_d$ , this process obscures the direct link between  $N_d$  and  $N_a$  associated with activation. The rather low  $ACI_N$  at Pt. Reyes could well reflect an active collision-coalescence process (even for nonprecipitating clouds) rather than a low activated fraction.

#### 4.2.2. Aerosol Size Distribution

[31] From the set of observations at Pt. Reyes we can examine the sensitivity of ACI to aerosol size through the Ångström exponent. Sensitivity of  $ACI_N$  when the data are sorted by values for  $\hat{a}$  is shown in Figure 7a. For  $\hat{a} > 1$ , indicative of smaller particles,  $ACI_N = 0.36$  is smaller than the  $ACI_N = 0.48$  for the aggregated data, as these smaller particles require higher supersaturations to activate. When larger particles only are considered,  $\hat{a} < 1$ ,  $ACI_N = 0.63$  is much higher than the aggregate value of 0.48.

#### 4.2.3. Updraft Velocity

[32] Sensitivity of  $ACI_N$  to cloud turbulence is shown in Figure 7b. Higher supersaturations as a result of stronger  $w$  account for greatly increased ACI values;  $ACI_N = 0.58$  for  $w > 0.5 \text{ m s}^{-1}$  and  $ACI_N = 0.69$  for  $w > 1.0 \text{ m s}^{-1}$ . This result is in accord with *Leitch et al.* [1996] and *Feingold et al.* [2003], who found a correlation of 0.67 between column maximum updraft and  $ACI_r$ . Other cloud dynamical effects or feedbacks may also affect the number of activated particles but are not considered here.

#### 4.2.4. Adiabaticity

[33] *Kim et al.* [2008] used a measure of cloud adiabaticity to represent entrainment-mixing processes in order to determine its effect on variability in cloud optical properties and aerosol-cloud interactions. That study showed that the albedo effect is more significant in adiabatic clouds. Determination of cloud adiabaticity requires cloud base temperature, a robust measurement of which is available at Pt. Reyes only from balloon-borne soundings every 6 h. Adiabaticity is calculated here for 1-h periods straddling the time of the relevant daytime soundings (typically 1730 UTC and 2330 UTC) within the available aggregate data

set. Figure 8 shows the relationship between adiabaticity,  $\beta$ , and  $ACI_r$ . Periods for which an ACI was calculated but the adiabaticity did not fall between 0 and 1.2 are shown as  $\beta = 0$ . A dependence is evident if all values for  $ACI_r$  are considered (all symbols); however, for results that fall within the  $ACI_r$  bounds between 0 and 0.33 (gray symbols) no dependence is evident. ACI values that do fall within these limits range from 0 to 0.28, almost the full theoretically plausible range. It is possible that since most of the clouds observed at Pt. Reyes are close-to-adiabatic, the sensitivity of ACI to adiabaticity is weak. Using such a limited data set to quantify aerosol-cloud interactions can also introduce error, leading to theoretically implausible results, as discussed in the next section.

### 4.3. Sensitivity of ACI to Scale and Resolution

#### 4.3.1. Effects of Observational Scale

[34] Consistently relating the optical and microphysical properties of aerosol and cloud requires knowledge of the scales over which the individual properties vary and how

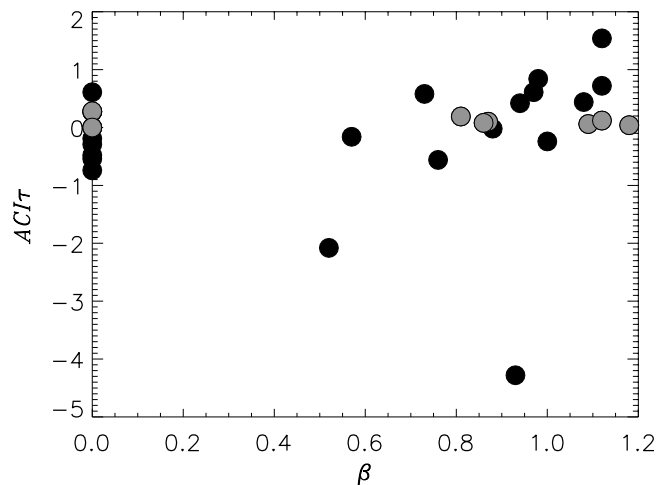


**Figure 8.**  $ACI_r$  calculated for 1-h segments around soundings as a function of adiabaticity  $\beta$ , where  $\beta$  is the ratio of LWP to the adiabatic LWP. Gray symbols represent physical results for  $ACI_r$  that fall between 0 and 0.33.

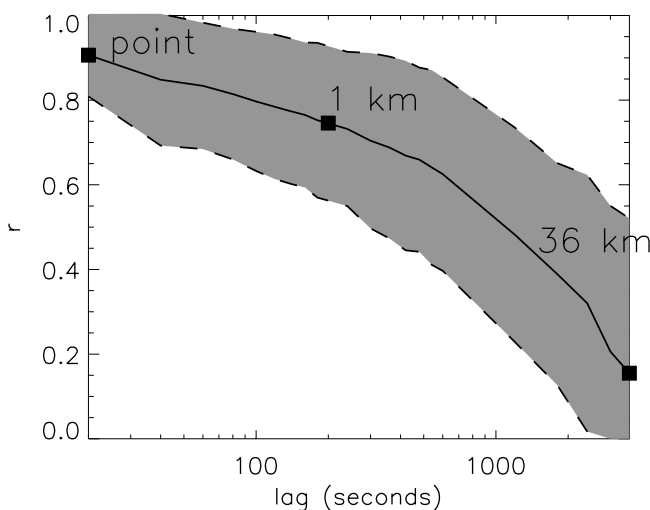


**Figure 9.** Lagged autocorrelation of LWP from the Pt. Reyes deployment for daily data. The solid line is the mean of the autocorrelations for all days and the shaded envelope depicts the standard deviation from the mean.

they relate to each other. The extent to which this variability is represented in observations of different scales and resolutions may affect analyses. For example, satellite-based observations such as MODIS are useful for regional- to global-scale monitoring of changes in cloud radiative properties and relevant climate processes that may not be practical from ground-based point measurements. However, their large footprint may incorporate clouds having a significant range in LWP. Estimates of ACI from satellite that ignore the constraint of constant LWP may result in large ACI uncertainty if variation in LWP is high.

[35] To illustrate the effect of scale on uncertainty in ACI estimates, we consider, theoretically, the relationship in scale between ground-based and satellite-based estimates of ACI. We use Taylor’s frozen field hypothesis that implies the equivalence of spatially and temporally lagged autocorrelations. Lag-autocorrelations using the same data from Figure 5a (i.e., including high LWP) are shown in Figure 9 for daily data over a range of lag times up to 1 h. The mean of the autocorrelations over all of the days is depicted by the solid line and one standard deviation from the mean is represented by the shaded envelope. The autocorrelation is overlain with the temporal equivalent of the ground-based spatial scale marked “point”, and satellite-based spatial scales of 1 km and 36 km. These spatial scales are defined using a  $5 \text{ m s}^{-1}$  wind velocity for a 1 km sensor pixel (MODIS equivalent). At the temporal (spatial) scale of a 200 s (1 km) pixel from space-based imagery (e.g., MODIS), there is a considerable amount of variability. The 36 km pixel denotes the point at which the autocorrelation reaches approximately zero.

[36] At the scale of the satellite-based observations, it is clear that averaging occurs over a wider range of LWP values than at the resolution of ground-based observations. The incorporation of data at larger spatial scales increases the chance of the occurrence of drizzle, which tends to have a spatial scale of 10 km in stratocumulus [Paluch and Lenschow, 1991]. This could result in significant reductions

in ACI, as demonstrated by Figures 4 and 5. On the other hand, if conditions over the scale of the satellite sensor resolution are homogeneous, averaging would not affect ACI in this manner. Many satellite-based analyses average finer-scale measurements (e.g., 0.5 to 1 km) to products of 150 km or greater [e.g., Chameides *et al.*, 2002; Kaufman *et al.*, 2005; Quaas and Boucher, 2005], incorporating data over larger scales than those represented with the ground-based observations here. The implications for model parameterizations based on space-based observations of ACI is that these parameterizations may tend to underestimate radiative forcing, as illustrated further in section 4.4.

#### 4.3.2. Variability in Aerosol

[37] The aggregate measures of ACI from this large sample of high temporal resolution observations made at Pt. Reyes produce results that are statistically robust. However, such data sets are rarely available, especially at a sufficient number of representative sites over the globe, and covering a diverse set of cloud types. Typically, observations at high temporal resolution are collected during short-term intensive observation periods at a single site, or satellite-based observations are used to obtain regional or even global-scale information with sacrifices in resolution. When data sets from the Pt. Reyes deployment with reduced scale and resolution are used, a high level of variability occurs in ACI measures.

[38] Figure 10 presents the ACI measures from equation (1) as in Figure 3 but for data from one day only, 3 September 2005 that is shown in Figure 1. As discussed in section 2, this day illustrates the albedo effect quite well. If we use the  $ACI_N$  value for reference, 0.51, the result is typical, and the consistency among the different measures found in the aggregate data set is maintained. The correlation coefficient for  $ACI_N$  is 0.5, an increase over that for the aggregate data, and the slopes of the ACI calculations are each significant at the 99% probability level according to the student’s *t* test. The majority of individual days from the Pt. Reyes deployment, however, do not produce results that are consistent with the aggregate data.

[39] Figure 11 shows the range of  $ACI_N$  calculated from daily data sets available from late June through September during the Pt. Reyes deployment.  $ACI_N$  is plotted as a function of the dispersion of aerosol data for that particular day, specifically the percent standard deviation  $\sigma$  of the mean  $\mu$  of the CCN concentrations,  $(\sigma/\mu)*100$ . Results that fall within theoretical bounds (0–1.0), indicated by the gray symbols, are obtained more frequently when the dispersion in the aerosol data is high enough for the effect on cloud microphysical properties to be detected. This reflects the fact that the calculation of  $ACI_N$  slopes is more robust when aerosol concentration exhibits a higher degree of variability. The range of  $ACI_N$  values within the physical limits of 0.0–1.0 is from 0.04 to 0.92. A large variability in  $N_{CCN}$  is, however, not a sufficient condition for theoretically reasonable values of ACI; there are a number of fairly large  $N_{CCN}$  standard deviation points associated with values of ACI less than zero and greater than one. As discussed earlier, failure to account for factors other than aerosol concentration such as aerosol size distribution, or physical processes such as advection, in addition to measurement and retrieval errors, may account for ACI values falling outside the range of these theoretical bounds.

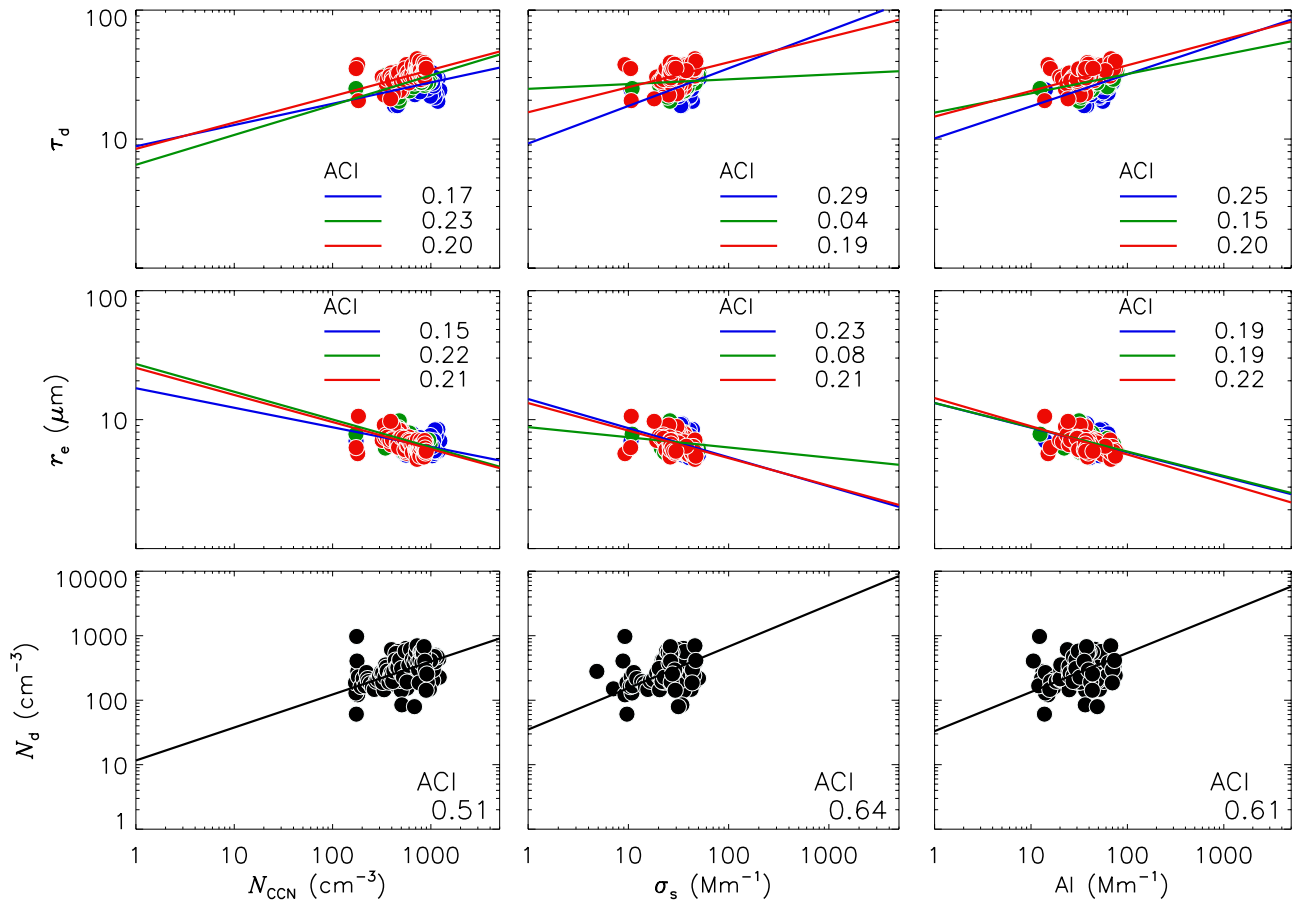


**Figure 10.** ACI measures for 3 September 2005 from equation (1) as in Figure 3. Cloud properties ( $\tau_d$ ,  $r_e$ ,  $N_d$ ) are derived from measurements made by the 2NFOV and MWR instruments, and aerosol properties ( $N_{CCN}$ ,  $\sigma_s$ , AI) are derived from ground-based in situ observations made by the AOS. Regressions are made for LWP bins geometrically increasing in size by 10% around an approximate mean LWP value ( $120 \text{ g m}^{-2}$ ) for the deployment. Regressions shown are for the following bins: blue  $107 \leq \text{LWP} < 118 \text{ g m}^{-2}$ ; green,  $118 \leq \text{LWP} < 130 \text{ g m}^{-2}$ ; and red,  $130 \leq \text{LWP} < 143 \text{ g m}^{-2}$ .

**4.3.3. Effect of Spatial/Temporal Aggregation**

[40] Several factors contribute to the difficulty in quantifying ACI with much accuracy for such small subsets of the data. For example, during the short time periods of 1 h near radiosonde soundings, the variability in measures of aerosol is typically very low and the response of cloud microphysical properties to changes in aerosol concentrations is difficult to detect. Cloud dynamical processes (e.g., a mixing of cloud microphysical properties advected into the view volume) may also be dominant during these short time periods, obscuring aerosol-cloud interactions. As illustrated in Figure 9, averaging observations of individual cloud properties over space and time can bias characterizations of aerosol-cloud interactions. Averaging over time may also reduce the magnitude of the association between aerosol and cloud properties by correlating aerosol and cloud properties that are not coincident in space or time. Cross correlations between drop number concentrations and aerosol properties, illustrated in Figure 12, are determined for the Pt. Reyes data for a time lag from 20 s to 30 min using a lag step of 20 s. The cross correlations fall off quickly over a period of 30 min. Averaging or sampling aerosol and cloud properties over longer periods of time will

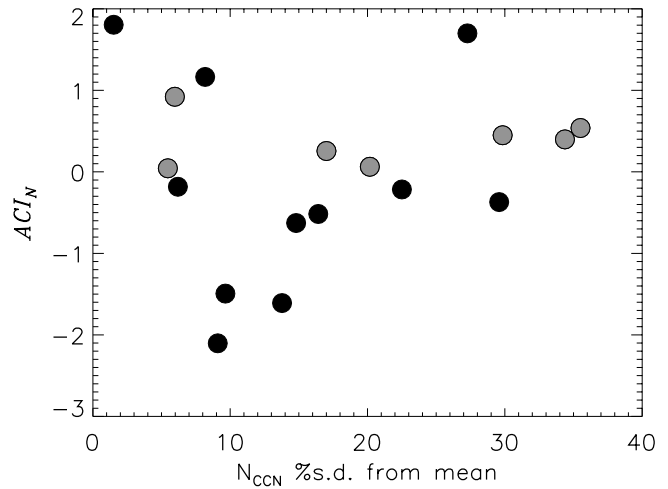


**Figure 11.**  $ACI_N$  calculated for daily data from the Pt. Reyes deployment available between late June and September as a function of aerosol concentration dispersion for that day. Gray symbols represent results that fall within the bounds of equation (1) for  $ACI_N$  (0–1).

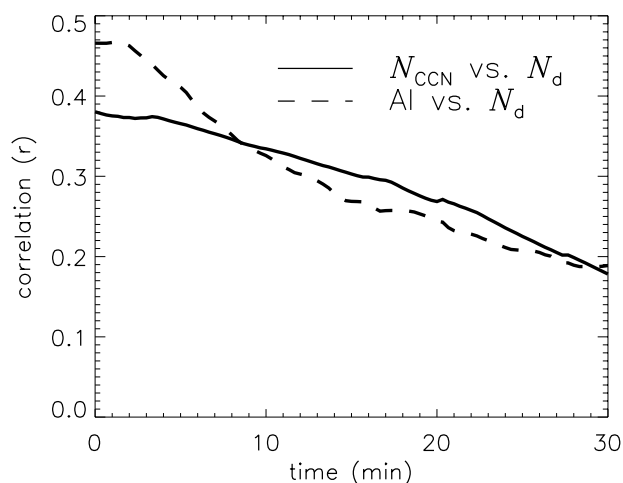


**Figure 12.** Cross correlations for aerosol properties versus drop number concentrations:  $N_{\text{CCN}}$  versus  $N_d$  and AI versus  $N_d$ . Correlations are calculated using a time lag step of 20 s over a time period from 20 s to 30 min.

result in lower sensitivity in detecting aerosol-cloud interactions and bias when calculating ACI. The choice of isolated or idealized events to characterize aerosol-cloud interactions may also bias results depending on the particular conditions, as shown in the range of ACI values presented throughout this paper. High temporal resolution observations are preferred as they represent the scale of relevant processes, but a large number of data points are required to account for the variability in calculated ACI due to the various factors discussed here. Therefore continued examination of such data sets over a wide range of climate regimes is needed to reduce uncertainty in the calculated radiative forcing of the albedo effect. Characterizing the factors driving variability in ACI will also provide for more appropriate ACI parameterizations.

#### 4.4. Implications for Radiative Forcing

[41] Estimates of the global radiative forcing of the albedo effect are routinely made by general circulation models (GCM), using parameterizations based on either empirical observations or physically based relationships that determine  $N_d$  from aerosol concentrations. Uncertainty in the forcing estimate is introduced into the model results as a function of uncertainty in the approach used to represent this relationship. For example, linear fits from satellite observations differ depending on the sensor type and resolution [e.g., Nakajima *et al.*, 2001; Lohmann and Lesins, 2002; Sekiguchi *et al.*, 2003] and deterministic relationships operating within coarse global-scale model grid cells do not represent with accuracy the variation across space in aerosol, cloud microphysical properties, and other factors such as updraft velocities that drive variation in aerosol-cloud interactions [Forster *et al.*, 2007]. We present the range in the local radiative forcing at Pt. Reyes that results from the range in ACI values determined above as a function of varying observational approaches or naturally varying aerosol and meteorological parameters. This allows for an indication of the relative importance and magnitude of these parameters in the uncertainty they produce in radiative forcing estimates.

[42] Local radiative forcing at the top of the atmosphere (TOA) is calculated for mean conditions over the Pt. Reyes deployment. Forcing is defined as the difference in TOA flux associated with an aerosol perturbation of  $N_{\text{CCN}} = 500 \text{ cm}^{-3}$  relative to  $N_{\text{CCN}} = 100 \text{ cm}^{-3}$ , the latter a concentration assumed to represent preindustrial conditions. Local forcing assumes complete (100%) cloud cover at a point and a cloud LWP of  $\sim 120 \text{ g m}^{-2}$ . Values of  $N_{\text{CCN}} = 500 \text{ cm}^{-3}$  and LWP =  $120 \text{ g m}^{-2}$  are approximate averages for the Pt. Reyes deployment (Figure 2). The curve in Figure 13 represents the change in the local TOA forcing as a function of the change in  $\text{ACI}_r$  (or  $\text{ACI}_s$ ) for these mean conditions. For example, an  $\text{ACI} = 0.05$  produces a forcing of  $-3.5 \text{ W m}^{-2}$  whereas an  $\text{ACI} = 0.15$  yields a forcing of  $-12.0 \text{ W m}^{-2}$ , a difference of  $8.5 \text{ W m}^{-2}$ . Other parameters assumed in the calculations were chosen to represent neutral solar conditions and other local conditions; the solar zenith angle is fixed at  $45^\circ$ , the radiative quantity represents the diurnal average of the fluxes on the equinox, the surface albedo is set at 0.15, and cloud base height at 300 m.

[43] The changes in local TOA forcing that result from the change in ACI due to the varying parameters illustrated in Figures 5–7 are summarized in Table 3. For the set of observations collected for coastal stratiform clouds during the Pt. Reyes deployment, neglecting to constrain ACI calculations by constant LWP, given a large LWP range ( $50 - 300 \text{ g m}^{-2}$  in this case), has the largest impact on radiative forcing, as discussed in section 4.3.1. This result has implications for using satellite observations to parameterize GCMs for aerosol-cloud interactions, with possible underestimation of the radiative forcing in conditions of appreciably varying LWP. Conversely, the implications of using surface remote sensing estimates of ACI versus airborne in situ estimates is a relatively small  $4.7 \text{ W m}^{-2}$ . Accounting for varying updraft velocity is important for determining the magnitude of the albedo effect and its

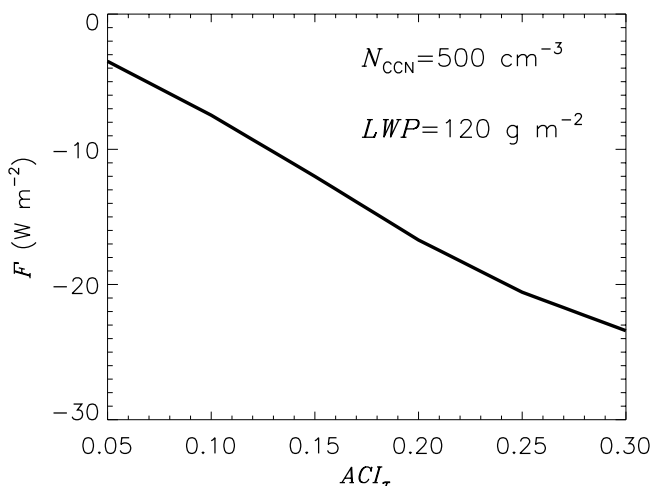


**Figure 13.** Local radiative forcing (100% cloud cover) for the change in ACI based on average aerosol concentrations and cloud liquid water at Pt. Reyes. Forcing is a diurnal average at the top of the atmosphere calculated as the difference in flux between cloud affected by  $N_{\text{CCN}} = 500 \text{ cm}^{-3}$  and  $N_{\text{CCN}} = 100 \text{ cm}^{-3}$ , the latter assumed as a background or preindustrial aerosol concentration.

**Table 3.** Range in Local TOA Radiative Forcing Resulting From the Ranges in Calculated ACI

Parameter	ACI Range (Form) <sup>a</sup>	RF Range (W m <sup>-2</sup> ) <sup>b</sup>
LWP binning (Figure 5)	0.06–0.16 (ACI <sub>r</sub> )	–4.3 to –13.0 (8.7)
$N_d$ retrieval (Figure 6)	0.43–0.56 (ACI <sub>N</sub> )	–11.1 to –15.8 (4.7)
Ångström exponent (Figure 7a)	0.14–0.19 (ACI <sub>r</sub> )	–9.3 to –17.5 (8.2)
	0.12–0.21 (ACI <sub>r</sub> )	
Updraft velocity (Figure 7b)	0.36–0.63 (ACI <sub>N</sub> )	–13.0 to –19.0 (6.0)
	0.16–0.23 (ACI <sub>r</sub> )	

<sup>a</sup>ACI is converted to form ACI<sub>r</sub> for ease of comparison to Figures 5–7 and 13. RF, radiative forcing.

<sup>b</sup>Change in RF.

radiative forcing, as well as aerosol size. Failure to consider these drivers in variability in ACI may result in errors in local radiative forcing of up to about 9 W m<sup>-2</sup> for the assumed aerosol perturbation at this site.

[44] The radiative forcing calculations presented here are intended to illustrate the relative magnitude and the order of magnitude of the different factors that result in variability in quantifying aerosol-cloud interactions. The absolute values of the forcing are strongly dependent on the concentrations chosen for the forcing definition, i.e., 500 cm<sup>-3</sup> and 100 cm<sup>-3</sup> as well as other model parameters such as solar geometry and surface albedo. Radiative forcing of the albedo effect for a broader range of conditions can be found in the work of *McComiskey and Feingold* [2008]. The results presented here represent local- to regional-scale conditions and cannot be simply extrapolated to a global average forcing. While global average forcing calculations typically result in smaller absolute values than those reported here [e.g., *Forster et al.*, 2007; *Lohmann et al.*, 2007], the same factors will contribute to uncertainty in calculating the radiative forcing of the albedo effect.

## 5. Summary and Conclusions

[45] In previous studies, measures of microphysical and optical responses of clouds to aerosol perturbations have been derived from a wide range of instrumentation and observational approaches, as well as over a range of climate regimes. Consequently, the range in measures is large and yields much uncertainty. Accurate quantification of the albedo effect requires an understanding of the uncertainties, biases, and drivers of variability in these measures.

[46] We have used a statistically robust data set for assessing aerosol effects on coastal stratiform clouds from the DOE ARM Pt. Reyes deployment on the California coast to examine variability in empirical measures of aerosol-cloud interactions (ACI) that result from different observational approaches and varying environmental conditions. The average ACI<sub>N</sub>(=  $d\ln N_d/d\ln \alpha$ ; equation (1)) for this data set is 0.48 with an  $r^2$  of 0.14, suggesting that changes in aerosol concentrations account for 14% of the variability observed in cloud microphysical properties. This finding is consistent with those from other regions that use ground-based observations to quantify ACI.

[47] Measures of ACI for coastal stratiform clouds based on cloud optical depth, drop size, and droplet concentration response to aerosol perturbations (equation (1)) show consistency among the different forms of ACI typically used to

quantify albedo effect. Depending on available observations, these forms can be substituted for one another. However, the use of ACI<sub>r</sub>(=  $\partial \ln \tau_d / \partial \ln \alpha|_{LWP}$ ) is recommended because it is closely related to albedo, and because it derives from independent measurements ( $\tau_d$  and  $\alpha$ ) and can therefore be unambiguously sorted by LWP. This is not true for ACI<sub>N</sub>(=  $\partial \ln r_e / \partial \ln \alpha|_{LWP}$ ) because  $r_e$  is calculated from  $\tau_d$  and LWP.

[48] Variability in ACI values has been characterized as a function of environmental and observational conditions. ACI was found to have a dependence on (1) the assumption of constant LWP, (2) the value of LWP, (3) methods for retrieving  $N_d$ , (4) aerosol size distribution, (5) updraft velocity, and (6) the scale and resolution of observations.

[49] From this assessment of ACI that employs a large set of high temporal resolution data from ground-based remote sensing the following key results emerge:

[50] 1. ACI based on ground-based measures of  $N_d$  are found to be consistent with in situ airborne measures for the MASE field experiment, suggesting that ground-based remote sensing can be used reliably when direct observations are not available, provided sufficiently large samples are available, and that aerosol size and composition are not strong determinants of ACI over the sampling period.

[51] 2. Use of various aerosol parameters that represent droplet activation, represented by  $\alpha$ , such as CCN concentration, light scattering, and aerosol index indicates that ACI based on the aerosol index produces similar results to those using CCN concentration. Use of light scattering alone, without aerosol size information, reduces the magnitude of ACI.

[52] 3. In agreement with earlier work, ACI increases with increasing updraft velocity.

[53] 4. ACI is lower in clouds with higher LWP. The latter have more active drop coalescence, which reduces  $N_d$  below the concentration of activated drops. Low values of ACI reflect the net effects of drop activation and collision-coalescence, rather than just activation, as is usually assumed. At high LWP (>~150 g m<sup>-2</sup>), the strong variability in ACI reflects precipitation scavenging of aerosol and therefore the effect of cloud on aerosol, rather than aerosol effects on clouds.

[54] 5. Averaging of ACI over large spatial domains tends to decrease ACI because of (1) degradation in correlation between aerosol and cloud fields at increasingly larger scales and (2) inclusion of LWP variability that inherently reduces ACI because of the probability of high LWP and high rates of drop collision-coalescence.

[55] 6. We do not see a clear dependence of ACI on liquid water content adiabaticity in the limited data set available here.

[56] The ACI<sub>N</sub> = 0.48 derived for the aggregate Pt. Reyes data set implies a local radiative forcing of approximately –13 W m<sup>-2</sup> (top-of-the-atmosphere) for the measured average CCN number concentration of 500 cm<sup>-3</sup> relative to an assumed 100 cm<sup>-3</sup> background. Implications of ACI variability for radiative forcing over broader parameter space (LWP and aerosol perturbation) can be found in the work of *McComiskey and Feingold* [2008].

[57] The above dependences of ACI measures on the context in which they are calculated has implications for developing parameterizations for modeling the albedo effect

and its radiative forcing on a global scale. Accounting for these factors will lead to more appropriate model parameterizations and more accurate estimates of the radiative forcing of the albedo effect. For example, parameterizations that are flexible with respect to updraft velocity rather than consisting of a single constraint for the number of activated cloud droplets would be more realistic. In the context of radiative forcing, variability in ACI due to these factors can cause differences in local forcing of approximately 5 to 9 W m<sup>-2</sup>, depending on the factor that is considered. Reported uncertainties need to take into consideration different approaches and/or observational platforms and parameterizations should be sensitive to variability in aerosol and other dynamical parameters. This is a preliminary exercise in reducing uncertainty in the radiative forcing of aerosol indirect effects by indicating parameters that produce variability in the quantification of ACI. Future efforts to quantify the albedo effect for radiative forcing calculations should address the factors shown here for conditions in different climate regimes and on a global scale in order to reduce that uncertainty.

[58] **Acknowledgments.** This work was supported by the Atmospheric Radiation Measurement Program of the U.S. Department of Energy Office of Science under grants DE-AI02-06ER64215, DE-FG02-06ER64167, DE-FG02-08ER64563, and DE-FG02-03ER63531.

## References

- Ackerman, A. S., M. P. Kirkpatrick, D. E. Stevens, and O. B. Toon (2004), The impact of humidity above stratiform clouds on indirect aerosol climate forcing, *Nature*, *432*, 1014–1017, doi:10.1038/nature03174.
- Albrecht, B. (1989), Aerosols, cloud microphysics, and fractional cloudiness, *Science*, *245*, 1227–1230, doi:10.1126/science.245.4923.1227.
- Anderson, T. L., D. S. Covert, J. D. Wheeler, J. M. Harris, K. D. Perry, B. E. Trost, D. J. Jaffe, and J. A. Ogren (1999), Aerosol backscatter fraction and single scattering albedo: Measured values and uncertainties at a coastal station in the Pacific Northwest, *J. Geophys. Res.*, *104*, 26,793–26,807, doi:10.1029/1999JD900172.
- Anderson, T. L., R. J. Charlson, D. M. Winker, J. A. Ogren, and K. Holmen (2003), Mesoscale variations of tropospheric aerosols, *J. Atmos. Sci.*, *60*, 119–136, doi:10.1175/1520-0469(2003)060<0119:MVOTA>2.0.CO;2.
- Barker, H. W. (2000), Indirect aerosol forcing by homogeneous and inhomogeneous clouds, *J. Clim.*, *13*, 4042–4049, doi:10.1175/1520-0442(2000)013<4042:IAFBHA>2.0.CO;2.
- Bennartz, R. (2007), Global assessment of marine boundary layer cloud droplet number concentration from satellite, *J. Geophys. Res.*, *112*, D02201, doi:10.1029/2006JD007547.
- Boers, R., J. A. Acarreta, and J. L. Gras (2006), Satellite monitoring of the first indirect aerosol effect: Retrieval of the droplet concentration of water clouds, *J. Geophys. Res.*, *111*, D22208, doi:10.1029/2005JD006838.
- Brenguier, J.-L., H. Pawlowska, and L. Schüller (2003), Cloud microphysical and radiative properties for parameterization and satellite monitoring of the indirect effect of aerosol on climate, *J. Geophys. Res.*, *108*(D15), 8632, doi:10.1029/2002JD002682.
- Bréon, F.-M., D. Tanre, and S. Generoso (2002), Aerosol effects on cloud droplet size monitored from satellite, *Science*, *295*, 834–838, doi:10.1126/science.1066434.
- Chameides, W. L., C. Luo, R. Saylor, D. Streets, Y. Huang, M. Bergin, and F. Giorgi (2002), Correlation between model-calculated anthropogenic aerosol and satellite-derived cloud optical depths: Indication of indirect effect?, *J. Geophys. Res.*, *107*(D10), 4085, doi:10.1029/2000JD000208.
- Chiu, J. C., A. Marshak, Y. Knayazikhin, W. J. Wiscombe, H. W. Barker, J. C. Barnard, and Y. Luo (2006), Remote sensing of cloud properties using ground-based measurements of zenith radiance, *J. Geophys. Res.*, *111*, D16201, doi:10.1029/2005JD006843.
- Conover, J. H. (1966), Anomalous cloud lines, *J. Atmos. Sci.*, *23*, 778–785, doi:10.1175/1520-0469(1966)023<0778:ACL>2.0.CO;2.
- Delene, D. J., and J. A. Ogren (2002), Variability and aerosol optical properties at four North American surface monitoring sites, *J. Atmos. Sci.*, *59*, 1135–1150.
- Dusek, U., et al. (2006), Size matters more than chemistry for cloud-nucleating ability of aerosol particles, *Science*, *312*, 1375–1378, doi:10.1126/science.1125261.
- Ervens, B., G. Feingold, and S. M. Kreidenweis (2005), The influence of water-soluble organic carbon on cloud drop number concentration, *J. Geophys. Res.*, *110*, D18211, doi:10.1029/2004JD005634.
- Feingold, G. (2003), Modeling of the first indirect effect: Analysis of measurement requirements, *Geophys. Res. Lett.*, *30*(19), 1997, doi:10.1029/2003GL017967.
- Feingold, G., L. A. Remer, J. Ramaprasad, and Y. Kaufman (2001), Analysis of smoke impact on clouds in Brazilian biomass burning regions: An extension of Twomey's approach, *J. Geophys. Res.*, *106*, 22,907–22,922, doi:10.1029/2001JD000732.
- Feingold, G., W. L. Eberhard, D. E. Veron, and M. Previdi (2003), First measurements of the Twomey aerosol indirect effect using ground-based remote sensors, *Geophys. Res. Lett.*, *30*(6), 1287, doi:10.1029/2002GL016633.
- Feingold, G., R. Furrer, P. Pilewskie, L. A. Remer, Q. Min, and H. Jonsson (2006), Aerosol indirect effect studies at Southern Great Plains during the May 2003 intensive operations period, *J. Geophys. Res.*, *111*, D05S14, doi:10.1029/2004JD005648.
- Forster, P., et al. (2007), Changes in atmospheric constituents and in radiative forcing, in *Climate Change 2007: The Physical Science Basis – Contribution of Working Group I to the Fourth Assessment Report of the Intergovernmental Panel on Climate Change*, edited by S. Solomon et al., pp. 289–348, Cambridge Univ. Press, New York.
- Garrett, T. J., C. Zhao, X. Dong, G. G. Mace, and P. V. Hobbs (2004), Effects of varying regimes on low-level Arctic stratus, *Geophys. Res. Lett.*, *31*, L17105, doi:10.1029/2004GL019928.
- Jefferson, A. (2005), *Aerosol Observing System (AOS) Handbook, ARM TR-014*, Off. of Sci., U.S. Dept. of Energy, Washington, D. C.
- Jiang, H., G. Feingold, and W. R. Cotton (2002), Simulations of aerosol-cloud-dynamical feedbacks resulting from entrainment of aerosol into the marine boundary layer during the Atlantic Stratocumulus Transition Experiment, *J. Geophys. Res.*, *107*(D24), 4813, doi:10.1029/2001JD001502.
- Kassianov, E., C. N. Long, and M. Ovtchinnikov (2005), Cloud sky cover versus cloud fraction: Whole-sky simulations and observations, *J. Appl. Met.*, *44*, 86–98, doi:10.1175/JAM-2184.1.
- Kaufman, Y., I. Koren, L. A. Remer, D. Rosenfeld, and Y. Rudich (2005), The effect of smoke, dust, and pollution aerosol on shallow cloud development over the Atlantic Ocean, *Proc. Natl. Acad. Sci. U. S. A.*, *102*(32), 11,207–11,212, doi:10.1073/pnas.0505191102.
- Kim, B.-G., S. E. Schwartz, M. A. Miller, and Q. Min (2003), Effective radius of cloud droplets by ground-based remote sensing: Relationship to aerosol, *J. Geophys. Res.*, *108*(D23), 4740, doi:10.1029/2003JD003721.
- Kim, G.-G., M. A. Miller, S. E. Schwartz, Y. Liu, and Q. Min (2008), The role of adiabaticity in the aerosol first indirect effect, *J. Geophys. Res.*, *113*, D05210, doi:10.1029/2007JD008961.
- Leitch, W. R., C. M. Banic, G. A. Isaac, M. D. Couture, P. S. K. Liu, I. Gultepe, S.-M. Li, L. Kleinman, J. I. MacPherson, and P. H. Daum (1996), Physical and chemical observations in marine stratus during the 1993 North Atlantic Regional Experiment: Factors controlling cloud droplet number concentrations, *J. Geophys. Res.*, *101*, 29,123–29,135, doi:10.1029/96JD01228.
- Liu, Y. G., and P. Daum (2002), Indirect warming effect from dispersion forcing, *Nature*, *419*, 580–581, doi:10.1038/419580a.
- Lohmann, U., and G. Lesins (2002), Stronger constraints on the anthropogenic indirect aerosol effect, *Science*, *298*, 1012–1015, doi:10.1126/science.1075405.
- Lohmann, U., P. Stier, C. Hoese, S. Ferrachat, S. Kloster, E. Roeckner, and J. Zhang (2007), Cloud microphysics and aerosol indirect effects in the global climate model ECHAM5-HAM, *Atmos. Chem. Phys.*, *7*, 3425–3446.
- Lu, M.-L., W. C. Conant, H. H. Jonsson, V. Varutbangkul, R. C. Flagan, and J. H. Seinfeld (2007), The Marine Stratus/Stratocumulus Experiment (MASE): Aerosol-cloud relationships in marine stratocumulus, *J. Geophys. Res.*, *112*, D10209, doi:10.1029/2006JD007985.
- Lubin, D., and A. Vogelmann (2006), A climatologically significant aerosol longwave indirect effect in the Arctic, *Nature*, *439*, doi:10.1038/nature04449.
- McComiskey, A., and G. Feingold (2008), Quantifying error in the radiative forcing of the first indirect effect, *Geophys. Res. Lett.*, *35*, L02810, doi:10.1029/2007GL032667.
- Miller, M. A., and A. Slingo (2007), The ARM Mobile Facility and its first international deployment: Measuring radiative flux divergence in West Africa, *Bull. Am. Meteorol. Soc.*, *88*, 1229–1244, doi:10.1175/BAMS-88-8-1229.

- Nakajima, T., A. Higurashi, K. Kawamoto, and J. E. Penner (2001), A possible correlation between satellite-derived cloud and aerosol microphysical parameters, *Geophys. Res. Lett.*, *28*, 1171–1174, doi:10.1029/2000GL012186.
- Paluch, I. R., and D. H. Lenschow (1991), Stratiform cloud formation in the marine boundary layer, *J. Atmos. Sci.*, *48*, 2141–2158, doi:10.1175/1520-0469(1991)048<2141:SCFITM>2.0.CO;2.
- Platnick, S., and S. Twomey (1994), Determining the susceptibility of cloud albedo to changes in droplet concentration with the Advanced Very High-Resolution Radiometer, *J. Appl. Met.*, *33*, 334–347, doi:10.1175/1520-0450(1994)033.
- Pruppacher, H. R., and J. D. Klett (1997), *Microphysics of Clouds and Precipitation*, 954 pp., Kluwer Acad., Dordrecht, Netherlands.
- Quaas, J., and O. Boucher (2005), Constraining the first aerosol indirect radiative forcing in the LMDZ GCM using POLDER and MODIS satellite data, *Geophys. Res. Lett.*, *32*, L17814, doi:10.1029/2005GL023850.
- Quaas, J., O. Boucher, and F.-M. Bréon (2004), Aerosol indirect effects in POLDER satellite data and the Laboratoire de Meteorologie Dynamique-Zoom (LMDZ) general circulation model, *J. Geophys. Res.*, *109*, D08205, doi:10.1029/2003JD004317.
- Ramanathan, V., et al. (2001), Aerosols, climate, and the hydrological cycle, *Science*, *294*, 2119–2124.
- Ramaswamy, V., et al. (2001), Radiative forcing of climate change, in *Climate Change 2001: The Scientific Basis—Contribution of Working Group I to the Third Assessment Report of the Intergovernmental Panel on Climate Change*, edited by J. T. Houghton et al., pp. 349–416, Cambridge Univ. Press, New York.
- Schwartz, S. E., Harshvardhan, and C. M. Benkovitz (2002), Influence of anthropogenic aerosol on cloud optical depth and albedo shown by satellite measurements and chemical transport modeling, *Proc. Natl. Acad. Sci. U. S. A.*, *99*(4), 1784–1789, doi:10.1073/pnas.261712099.
- Sekiguchi, M., T. Nakajima, K. Suzuki, K. Kawamoto, A. Higurashi, D. Rosenfeld, I. Sano, and S. Mukai (2003), A study of the direct and indirect effects of aerosols using global satellite data sets of aerosol and cloud parameters, *J. Geophys. Res.*, *108*(D22), 4699, doi:10.1029/2002JD003359.
- Sheridan, P. J., D. J. Delene, and J. A. Ogren (2001), Four years of continuous surface aerosol measurements from the Department of Energy's atmospheric radiation measurement program Southern Great Plains cloud and radiation testbed site, *J. Geophys. Res.*, *106*, 20,735–20,747, doi:10.1029/2001JD000785.
- Stephens, G. L. (1978), Radiation profiles in extended water clouds I: Theory, *J. Atmos. Sci.*, *35*, 2111–2122, doi:10.1175/1520-0469(1978)035<2111:RPIEWC>2.0.CO;2.
- Stevens, B., W. R. Cotton, G. Feingold, and C.-H. Moeng (1998), Large-eddy simulations of strongly precipitating, shallow, stratocumulus-topped boundary layers, *J. Atmos. Sci.*, *55*, 3616–3638.
- Turner, D. D., S. A. Clough, J. C. Liljegren, E. E. Clothiaux, K. Cady-Pereira, and K. L. Gaustad (2007), Retrieving liquid water path and precipitable water vapor from Atmospheric Radiation Measurement (ARM) microwave radiometers, *IEEE Trans. Geosci. Remote Sens.*, *45*, 3680–3690, doi:10.1109/TGRS.2007.903703.
- Twohy, C. H., et al. (2005), Evaluation of the aerosol indirect effect in marine stratocumulus clouds: Droplet number, size, liquid water path, and radiative impact, *J. Geophys. Res.*, *110*, D08203, doi:10.1029/2004JD005116.
- Twomey, S. (1959), The nuclei of natural cloud formation. Part II: The supersaturation in natural clouds and the variation of cloud droplet concentration, *Geophys. Pure Appl.*, *43*, 243–249.
- Twomey, S. (1974), Pollution and the planetary albedo, *Atmos. Environ.*, *8*, 1251–1256, doi:10.1016/0004-6981(74)90004-3.
- Twomey, S. (1977), The influence of pollution on the shortwave albedo of clouds, *J. Atmos. Sci.*, *34*, 1149–1152, doi:10.1175/1520-0469(1977)034<1149:TIOPT>2.0.CO;2.
- Wang, S., Q. Wang, and G. Feingold (2003), Turbulence, condensation and liquid water transport in numerically simulated nonprecipitating stratocumulus clouds, *J. Atmos. Sci.*, *60*, 262–278.
- Xue, H., and G. Feingold (2006), Large-eddy simulations of trade wind cumuli: Investigations of aerosol indirect effects, *J. Atmos. Sci.*, *63*, 1605–1622, doi:10.1175/JAS3706.1.

J. C. Chiu, JCET, UMBC, Suite 320, 5523 Research Park Drive, Baltimore, MD 21228, USA.

G. Feingold and A. McComiskey, CSD-2, Earth System Research Laboratory, NOAA, 325 Broadway, Boulder, CO 80305, USA. (allison.mccomiskey@noaa.gov)

A. S. Frisch, Cooperative Institute for Research in the Atmosphere, Colorado State University, Fort Collins, CO 80523-1375, USA.

M. A. Miller, Department of Environmental Sciences, Rutgers University, 14 College Farm Road, Room 243, New Brunswick, NJ 08901, USA.

Q. Min, Atmospheric Sciences Research Center, State University of New York at Albany, 251 Fuller Road, Albany, NY 12203, USA.

J. A. Ogren, GMD, Earth System Research Laboratory, NOAA, 325 Broadway, Boulder, CO 80305, USA.

D. D. Turner, Space Science and Engineering Center, University of Wisconsin-Madison, 1225 West Dayton Street, Madison, WI 52706, USA.